energies

MDPI

Article

Numerical Study on the Effect of Lambda Value (Oxygen/Fuel Ratio) on Temperature Distribution and Efficiency of a Flameless Oxyfuel Combustion System

Mersedeh Ghadamgahi [1,2,*], Patrik Ölund [1], Nils Å. I. Andersson [2] and Pär Jönsson [2]

[1] Ovako Sweden AB, 81382 Stockholm, Sweden; patrik.olund@ovako.com
[2] KTH Royal Institute of Technology, 11428 Stockholm, Sweden; nilsande@kth.se (N.Å.I.A.); parj@kth.se (P.J.)
* Correspondence: mersedeh.ghadamgahi@ovako.com or mersedeh@kth.se; Tel.: +46-70-717-68-34

Academic Editor: Mejdi Jeguirim
Received: 11 January 2017; Accepted: 1 March 2017; Published: 9 March 2017

Abstract: The flameless oxyfuel combustion technology has been proven to be a promising new method to reduce the fuel consumption and pollutants in industrial applications. Although this technology is widely used in industrial furnaces, a lack of understanding exists about the effect of the controlling parameters on the final operational conditions is tangible. In this study, a validated computational fluid dynamics (CFD) model is used to simulate six cases of flameless oxyfuel combustion burners with different lambda values (ratio of oxygen/fuel mass flow rates). The CFD model uses the steady laminar flamelet model (SLFM) to solve the probability density function (PDF) for combustion, the discreet ordinates (DO) radiation model with the weighted sum of the gray gases model (WSGGM) to solve radiation, and the realizable k-ε to model the turbulence. It is seen that an increased oxygen injection velocity due to an increased lambda value increases the exhaust losses, but produces a larger volumetric flame. This leads to a more uniform temperature distribution. The total temperature difference in a case with a λ value of 1.02 is reported to be 272 (14.9%), while the amount for a case with a λ value of 1.2 is 67 (4.7%). This effect is further explained by introducing a new definition value for the furnace efficiency that includes both the thermal and production losses.

Keywords: computational fluid dynamics (CFD); flameless oxyfuel; combustion; lambda value; soaking pit furnace

1. Introduction

The oxyfuel combustion technology was introduced in the late eighties to target the increasing demand for controlling the CO_2 and NO_x production in industrial combustion systems. In this technology, the fuel is combusted in an almost pure oxygen atmosphere instead of using air. This provides the mean for a CO_2 sequestration from the flue gases [1]. This combustion technology was initially promoted and studied for the usage in coal-fired power plants and coal-combustion applications [2,3]. Later on, this technology became rapidly popular for use in other applications, as academic attention was also attracted to the subject in order to provide a better understanding and to develop modification methods [4]. In addition, fundamental research was carried out by Argonne National Laboratory (ANL) with the study on a pilot scale furnace equipped with an oxyfuel burner [5–7]. Later, the International Flame Research Foundation (IFRF) carried out major research in this area, with usage of an oxy-coal combustor with a flue gas recirculation (FGR) system.

In 2005, Buhre et al. [2] highlighted the importance of employing oxyfuel systems as an approach for CO_2 sequestration. They provided a comprehensive research review of previous work that had been carried out as well as the status of the technology at that time. In the same year, Wall et al. [8] pointed out the importance of the role of recycled flue gases inside the combusting chamber. They

claimed that these can control the flame temperature and compromise the lack of the flue gas volume (N_2) in an oxyfuel system. In 2007, the flame stability and NO_x emissions from oxy-fuel combustion was investigated by Kim et al. [9], in an experimental study. The system in this study was also equipped with a FGR system. They reported that the oxyfuel combustor has the best flame stability. Another experimental work was done by Andersson et al. [10] which investigated the combustion chemistry in air-fuel and oxyfuel combustion systems. The study was done on a 100 kW test unit and the results showed that oxyfuel produces up to 30% less NO_x emissions compared to an identical air-fuel combustion system. In 2010, Toftegaard et al. [11] performed an extensive literature study on the subject of oxyfuel combustion. They concluded that a large lack of research exists in both pilot and plant testing on the issues related to oxyfuel combusting systems. A more extensive literature survey about oxyfuel combustion is presented in the work by Ghadamgahi et al. [12] and Wall et al. [13].

In the meantime, while many theoretical and laboratory studies were carried out on the subject, the fast development of computational simulations led to a new trend of using them to study the complicated issues related to combustion. Examples of the numerical studies on oxy-fuel combustion systems are given in references [14–16]. The focus of these studies was to develop and validate the proper computational models for combustion and radiation. More specifically, Johansson et al. [14] compared four different radiation models to study the accuracy and the relevance of using them to simulate an oxy-fired boiler. They reported that the weighted sum of the gray gases model (WSGGM) was the most accurate model to use for these applications. In 2012, Hjärtstam et al. [15] used the measured data of a 100 kW oxyfuel unit to investigate the effect of a non-gray radiation model on the predicted results. They reported that the non-gray model predicts acceptable results. Additionally, the SLFM combustion model was employed in this work, regarding the work done by Galletti et al. [17], and Ghadamgahi et al. [12]. In 2013, Galletti et al. [17] compared the predicted results from computational fluid dynamics (CFD) calculations for an oxy-natural gas combustion system, to the experimental results of a 3 MW semi-industrial furnace. They observed that the sub model, which considered a fast chemistry, was inaccurate for predicting the temperature magnitudes. Also, Ghadamgahi et al. [12] compared the predicted results from two CFD models, with and without chemical equilibrium, with experimental data, and the latter showed a better agreement [12]. A turbulence model of realizable k-ε was used according to the works by Liu et al. [18] and Ghadamgahi et al. [12]. Also, in 2016 Aziz et al. [19] used the k-ε turbulence model to investigate the palm kernel shell (PKS) co-firing of a 300 MWe pulverized coal-fired power plant [19]. It is also mentioned in the work by Filipponi et al. [20] that the realizable k-ε model gives more accurate results compared to the results from standard k-ε [20].

According to the literature above, one can consider the bullet points below as the main known advantages of oxyfuel combustion systems:

- An increased combustion efficiency
- Reduced CO_2 emission
- A higher flame temperature

Although, with increasing the usage of this technology some operational issues were also noticed. Examples of research that pointed out these issues were done by Buhre et al. [2] and Fredriksson et al. [21]. In Buhre et al. [2], the authors identified some problems associated with the use of oxyfuel combustion with respect to heat transfer, flame stability, and gaseous emissions. In addition, Fredriksson et al. [21] investigated the effect of air infiltration into the chamber, on the total NO_x formation. They reported that the sharp temperature gradient in the flame area produces a large amount of NO_x in the case of air infiltration. This consequently leads to a non-uniform scale formation on the slabs.

One of the modified versions of the conventional oxyfuel systems was the flameless oxyfuel combustion systems [4]. These systems also use pure oxygen as the oxidant, but the difference to normal oxyfuel burners is the use of a special burner design and a high (near-sonic) injection velocity

for both fuel and oxygen. The design of the burner, including the diameter and distance of the nozzles, promotes a high internal flue gas recirculation (IFGR) [4,22]. In the case of correct adjustments, the result is the production of a volumetric strained flame with a spread temperature distribution and a low concentration of oxygen and nitrogen inside the combustion chamber [22].

Shortly after the commercialization of this technology, it became a common practice in many steel industries, such as in walking beam and catenary furnaces at Outokumpu (Sweden) in 2003 [4], nine soaking pit furnaces at Arcometal (France) in 2005 [4], a rotary heart furnace in ArcelorMittal Shelby (OH, USA) in 2007 [4] and soaking pit furnaces in Ovako Sweden AB, in Hofors (Sweden) [4]. Beside these applications, a few academic studies were also performed to provide a better understanding of the practical issues and modeling tools. In 2006, Vesterberg et al. [23] listed the most important findings they observed by studying 10 full-scale industrial users of the flameless oxyfuel technique in reheating and annealing furnaces. Those are: a more uniform heating process, shorter heating cycles, and ultra-low emissions of NO_x even with the existence of ingress air. In the work by Krishnamurthy at al. [24] different burner types, such as flameless oxyfuel burners and high temperature air combustion (HiTAC) burners, were evaluated with respect to their thermal efficiency, inflame temperature distribution, heat flux, gas composition, and NO_x emissions for different levels of in-leakages of air. They concluded that the flameless burners provide a higher energy utilization efficiency, and a better temperature uniformity and heat flux profile, compared to traditional burners.

In 2007, Krishnamurthy et al. [25] used a semi-industrial furnace to investigate the NO_x formation for flameless oxyfuel combustion. They examined different burners, including a flameless oxy-propane burner to provide a comparative end-result. The comparisons show many advantages of using the flameless oxyfuel burners in comparison to traditional burners, such as a lower NO_x formation and a better temperature uniformity [25]. Later in 2016, Ghadamgahi et al. [12] used the experimental data from Krishnamurthy et al. [25] to compare three different CFD models and to validate the predictions for simulations of a flameless oxyfuel combustion [12]. These models were later used to simulate a full-scale soaking pit furnace and the predicted results were compared with experimental results presented by Ghadamgahi et al. [26].

Although these few studies were very useful to help understand and model the complicated case of using the flameless oxy-fuel technique, there is a large lack of studies on the role of operational parameters on the functioning condition of these burners. This is especially essential for industrial applications; to understand the effect of important operational parameters, such as the oxygen/fuel (lambda), efficiency, and temperature profile, on the combustion performance.

In this study, the validated models from the work by Ghadamgahi et al. [12,26] are used to simulate a full-size soaking pit furnace containing ingots, since the differences in the geometries is negligible. Simulations have been performed for six cases, using different magnitudes of the lambda value (inlet oxygen values). The validation was previously performed by comparing the predicted results with those taken from the experiments on a soaking pit furnace, equipped with a flameless oxyfuel burner, in Ovako Sweden AB [26]. The results from these simulations are used to compare these cases and to investigate the effect of the lambda value on the operational condition of a furnace when using a flameless oxyfuel combustion. Thus, to link an easy controlled parameter to temperature uniformity is of great practical value for the industry. In addition, a new definition of furnace efficiency is proposed. It considers the operational costs of a furnace besides the thermal costs. These operational costs are solely due to the design and operational conditions of the furnace.

2. Mathematical Models

A 3-dimensional mathematical model was developed to simulate the combustion in Ansys Fluent 16.0 (Producs 16, Ansys, Inc., http://www.ansys.com/). The following assumptions were considered to solve the problem:

- The flue gas mixture was assumed to behave like a perfect gas mixture.
- The condition was assumed to be steady state and therefore independent of time.

- The Lewis number for all the gas species was assumed to be one.
- The flow was assumed to be fully turbulent.
- The diffusion coefficients for all the gaseous products were assumed to be equal.
- All the external forces, except the gravity, were neglected.
- The flow was assumed to be incompressible in the chamber.
- Infiltration of air was assumed to be negligible and NO_x products were ignored.
- Combustion was assumed departed from the chemical equilibrium.
- A second-order upwind discretization scheme was used to solve the governing equation.

The governing equations were solved according to the assumptions above. Specifically these equations are:

Continuity equation:

$$\nabla.(\rho \mathbf{u}) = 0 \tag{1}$$

Momentum equation:

$$\nabla \cdot (\rho\, \mathbf{u}\, \mathbf{u}) = -\nabla p + \nabla.(\bar{\bar{\tau}}) + \rho g \tag{2}$$

Energy balance equation:

$$\rho c_p \mathbf{u}.\nabla T = \nabla.(k \nabla T) + S_h \tag{3}$$

where $\mathbf{u}$ is the velocity vector (m/s), ρ is the density (kg/m^3) and $\bar{\bar{\tau}}$ is the stress tensor. Furthermore, ρg and p are the gravitational body forces and the pressure (Pa), respectively. In addition, k represents the thermal conductivity (W/m·K), and c_p defines the heat capacity at a constant pressure (J/kg·K) [26]. Also S_h counts for any volumetric heat sources.

Regarding the incompressible behaviour of the flow, the Navier Stokes equation is solved, which can be written as follows:

$$(\mathbf{u}.\nabla)\mathbf{u} - \nu \nabla^2 \mathbf{u} = -\nabla \omega + g \tag{4}$$

where the parameter g represents the gravity and ω is thermodynamic work on the system. Furthermore, the parameter $\nu = \frac{\mu}{\rho}$ is the kinematic viscosity.

The realizable k-ε turbulence model was used to solve the Navier-Stokes equations and to model the turbulence. The validity of this sub-model for such problems is intensely argued in the work by Ghadamgahi et al. [12]. The turbulent kinetic energy (k) and the turbulent dissipation rate (ε) were solved as shown in Equations (5) and (6):

$$\frac{\partial(\rho k)}{\partial t} + \frac{\partial(\rho k u_i)}{\partial x_i} = \frac{\partial}{\partial x_j}\left(\mu + \frac{\mu_t}{\sigma_k}\right)\frac{\partial k}{\partial x_j} + G_k + G_b - \rho\varepsilon \tag{5}$$

$$\frac{\partial(\rho \varepsilon)}{\partial t} + \frac{\partial(\rho \varepsilon u_j)}{\partial x_j} = \frac{\partial}{\partial x_j}\left[\left(\mu + \frac{\mu_t}{\sigma_\varepsilon}\right)\frac{\partial \varepsilon}{\partial x_j}\right] + \rho\, C_1 S_\varepsilon - \rho C_2 \frac{\varepsilon^2}{k + \sqrt{\nu\varepsilon}} + C_{1\varepsilon}\frac{\varepsilon}{k} C_{3\varepsilon} G_b \tag{6}$$

where $C_1 = \max\left[0.43, \frac{\eta}{\eta+5}\right]$, $\eta = S\frac{k}{\varepsilon}$, $S = \sqrt{2 S_{ij} S_{ij}}$.

And $\sigma_k = 1.0$, $\sigma_\varepsilon = 1.2$, $C_2 = 1.9$, $C_{1\varepsilon} = 1.44$, and $C_{3\varepsilon}$ is described by Equation (7).

$$C_{3\varepsilon} = \tanh\left|\frac{v_\parallel}{u_\perp}\right| \tag{7}$$

According to the configuration of the burner, a non-premixed combustion with the mixture fraction (f) is considered. The mixture fraction is introduced as follows:

$$f = \frac{Z_i - Z_{i,ox}}{Z_{i,fuel} - Z_{i,ox}} \tag{8}$$

where Z_i stands for the ith species mass fraction and the subscript *ox* and *fuel* stand for the oxidizer stream and fuel stream, respectively. The combustion is calculated by using the SLFM to solve the PDF. This model considers the non-equilibrium effects of the combustion. This selection of a sub-model for reaching an accurate prediction for combustion is explained and argued in the work by Ghadamgahi et al. [12]. In this approach, the thermochemistry parameters are a function of the mixture fraction and the strain rate or Dissipation rate (χ):

$$\chi = 2D|\nabla f\ |^2 \tag{9}$$

where D is the diffusion coefficient.

Therefore, the following formulation is used to calculate the thermochemical parameters:

$$\overline{\Phi} = \iint \Phi(f, \chi_{st}) p(f, \chi_{st})\ \mathrm{d}f\ \mathrm{d}\chi_{st} \tag{10}$$

where Φ represents the species mass fractions and temperature while χ_{st} represents the stoichiometric dissipation rate [12].

For modeling the radiation, the DO radiation model with the WSGGM is used to solve the general radiative transfer equation (RTE). The set-up for using this method for the special case of oxy-fuel has been widely investigated in the literature [14,16,27–29].

The RTE over the radiative path of S and a spectral averaging over a band k is described as follows:

$$\overline{I}_{\nu_{k,n}} = \overline{I}_{\nu_{k,0}} \overline{\tau}_{\nu_{k,0\to n}} + \sum_{i=0}^{n-1} (\overline{\tau}_{\nu_{k,i+1\to n}} - \overline{\tau}_{\nu_{k,i\to n}}) \overline{I}_{b\nu_{k,\ i+\frac{1}{2}}} \tag{11}$$

where the over-bar stands for a spectral average over a band k, the index i refers to the spatial discretization, and $\overline{\tau}_{\nu k}$ can be expressed as follows:

$$\overline{\tau}_{\nu k} = 1 - \overline{a}_{\nu k} \tag{12}$$

where $\overline{a}$ is the absorption coefficient [12].

3. Materials and Methods

3.1. Furnace Geometry and Configuration

In the production line of bars and billets in Ovako Sweden AB (Figure 1), soaking pit furnaces are used to reheat the cast ingots prior to the rolling process [26]. The quality of the soaking process is essential, since it highly determines the final quality and mechanical properties of the steel. This process also strongly affects the operational conditions of the rolling mills. In Ovako Sweden AB, in Hofors, these furnaces are all equipped with flameless oxy-fuel burners, which use propane as fuel.

Each furnace is made of four cells, where each of them accommodates six ingots during the soaking process. Ingots, which are 4.2 tons each, are inserted into the cells by using the automatic hooks (Figure 2), regarding the desirable soaking time and soaking temperature for each steel grade. This soaking temperature for most of the cases is around 1200 °C, which needs to be applied in a uniform fashion [26].

Each cell has a rectangular shape as is shown in Figure 3 with the corresponding dimensions. Figure 3 also shows the arrangement and configuration of the ingots. Each cell is equipped with a flameless oxy-fuel burner with an adjustable oxygen and fuel injection velocity. The exhaust outlet is mounted on the same wall as the burner in order to promote a better flue gas circulation. A permanently located thermocouple is mounted 400 mm below the burner, which reports the state of temperature to the control system of the furnace. This thermocouple is located inside a long tube of 976 mm, which is mounted 345 mm into the wall and almost 630 mm inside the chamber. The refractory walls are made

of 230 mm AK60 A, 115 mm Porosil, and Skamolex 1100 in 450 and 200 mm at the transverse and longitudinal walls, respectively. The fuel is LPG No. 95, and its properties are given in Table 1 [26].

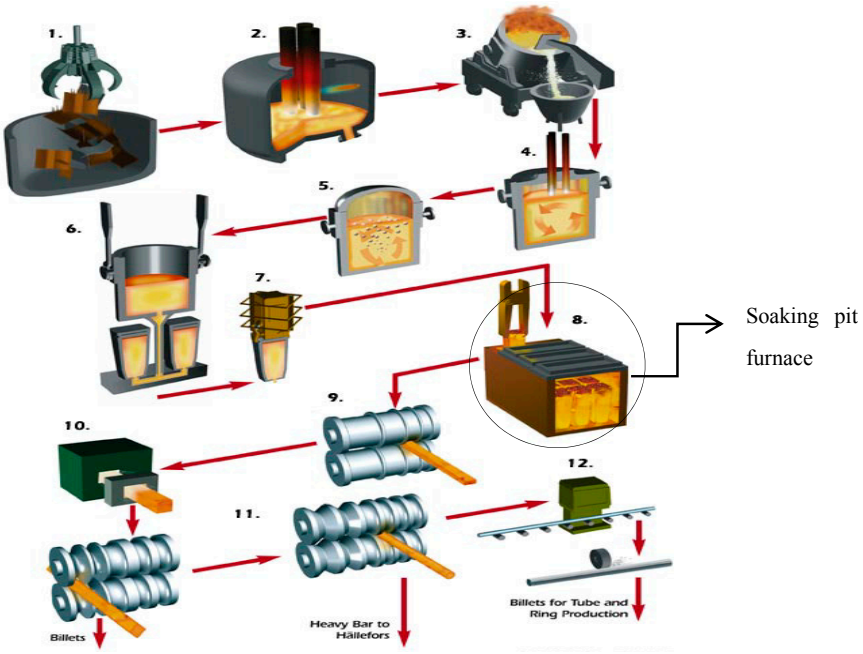

Figure 1. The production route of bars at Ovako Sweden AB, Hofors, Sweden [26].

Figure 2. The insertion of the ingots inside the soaking pit furnace.

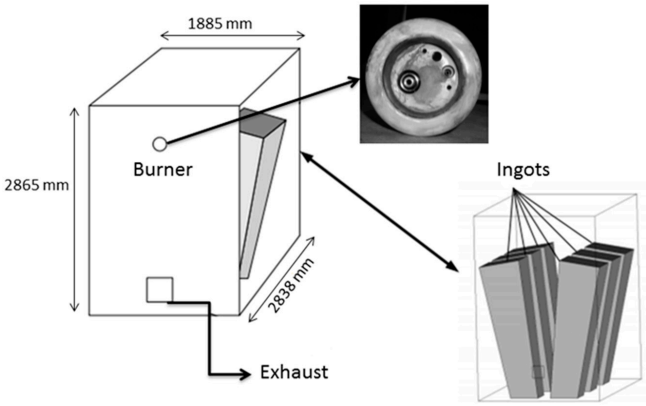

Figure 3. Soaking pit furnace configuration and arrangement of ingots inside the furnace [26].

Table 1. Propane properties.

Characteristics	Typical Data	Production Specification	Testing Method
Vapor Pressure 40 °C	1300	Max 1570	ASTM
Elemental Sulfur	<1 (mg/kg)	Max 5	SMS 378/282
Total Sulfur	<2 (mg/kg)	Max 10	ASTM D2784
Evaporation residue	5 (mg/kg)	Max 20	SMS 1513
Heavy pentanes	0	Min 95	-

3.2. Design of the Experiment

The detail of the experimental procedure, which has been used previously in the work of Ghadamgahi et al., can be found in [26]. In this experimental work, the local temperature is measured with shielded S-type thermocouples at two different levels, namely High and Low, inside the chamber. The thermocouples are inserted from the lid, through small holes that were considered for insertion, as shown in Figure 4. The exact locations of the thermocouples' probes are given in Table 2.

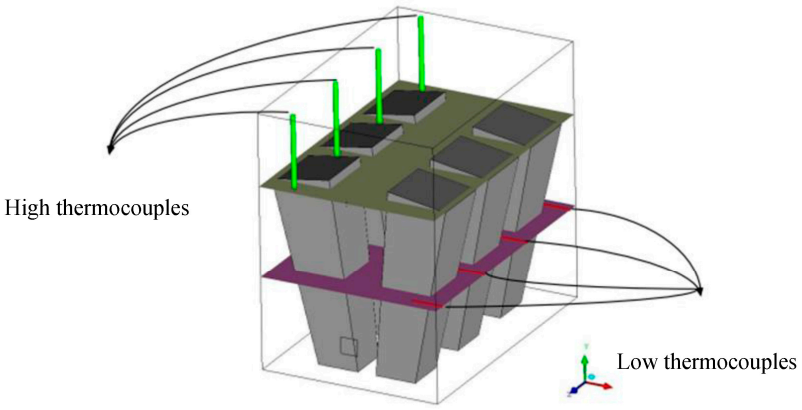

Figure 4. Arrangement of thermocouples in the soaking pit furnace [26].

Table 2. Coordinates of the S-type thermocouples inside the soaking pit furnace.

Thermocouple	Reference thermocouple	Low 1	High 1	Low 2	High 2	Low 3	High 3	Low 4	High 4
x (mm)	910	1487	514	1487	514	1487	514	1487	514
y (mm)	1105	1065	2065	1065	2065	1065	2065	1065	2065
z (mm)	0	2631	2631	1810	1810	987	987	246	246

3.3. Domain

The geometry and mesh were designed and drawn by using ICEM 13 (Producs 16, Ansys, Inc., http://www.ansys.com/), and imported to Ansys Fluent, as is shown in Figure 5. The arrangement of the ingots is simplified in this study, considering them as standing inside the chamber. This assisted with the lower cost for convergence and with the lower amount of mesh nodes. The asymmetric configuration of the burner requires a complete domain for the geometry of the whole furnace. The grid independency was investigated by comparing the results from different mesh set-ups, namely by using tetragonal and hexagonal meshes. The best compromise regarding both the convergence costs and accuracy was selected. This was the unstructured tetrahedron for the fluid domain. This is due to the fact that the tetragonal mesh with 850,000 nodes showed 12% better agreement for temperature at the controlling thermocouple probe, compared to the hexagonal mesh with 752,000 nodes. Also, the mesh structure was fine-tuned by adding the O-grid for the inlet of fuel and oxygen part. Also, the minimum orthogonal quality was 0.84, which is adequate according to the previous results presented [12,26].

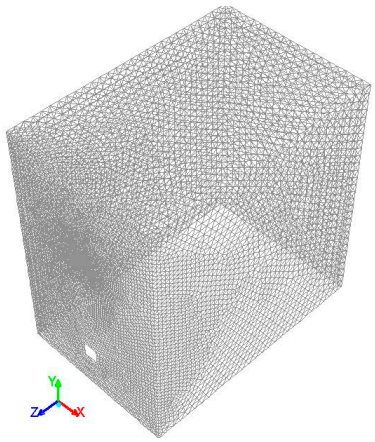

Figure 5. The mesh structure.

4. Boundary Conditions

The details of the inlet boundary conditions used for different cases of study, with different oxygen/fuel ratios (lambda value), are shown in Table 3.

Table 3. Inlet boundary condition for the different cases in this study.

Case Number	Inlet Fuel Rate (kg/s)	Inlet Oxygen Rate (kg/s)	λ	Burner Capacity (kW)
Case 1	0.013	0.0448	0.95	596
Case 2	0.013	0.0471	1.00	596
Case 3	0.013	0.0481	1.02	596
Case 4	0.013	0.0495	1.05	596
Case 5	0.013	0.0519	1.10	596
Case 6	0.013	0.0566	1.20	596

The inlet temperatures for propane and oxygen are 22 °C and 25 °C, and the hydraulic diameter is 7 mm and 5 mm, respectively, for all the cases. Furthermore, the turbulent intensity was calculated to be 6% and 5% for propane and oxygen inlets, respectively. The exterior walls are treated as a heat sink with a fixed heat flux, which is computed based on the specific material of each wall. These data are shown for each wall in Table 4 [26].

Table 4. Heat flux boundary condition parameters for the exterior walls [26].

Layer	Bottom	Longitudinal Wall	Transversal Wall	Lid
Heat loss (W/m^2)	530	450	500	650

The boundary condition on the ingots was a constant heat flux to the ingots. The calculation process of this magnitude that was done separately for each ingot is extensively explained in [26]. These magnitudes are shown in Table 5 [26].

Table 5. Wall boundary conditions for the ingots [26].

Ingot	Heat Flux (kW/m^2)
Ingot 1 (Front-right)	56.7
Ingot 2 (Middle-right)	43.7
Ingot 3 (Rear-right)	61
Ingot 4 (Front-left)	45.2
Ingot 5 (Middle-left)	48.4
Ingot 6 (Rear-left)	65.1

The boundary condition for the outlet is set as a "pressure outlet" condition in the chimney.

5. Results and Discussion

5.1. Experiment

The CFD model and sub-models used in this study have been validated by Ghadamgahi et al. [12,26] to simulate the full-scale soaking pit furnace. The simulation has been done according to the real operational condition of the furnace in the rolling mill, with a 596 kW burner capacity and a lambda value of 1.54. Furthermore, the mass flow rate for oxygen and propane injection was 0.06 and 0.013 kg/s, respectively. The maximum deviations between the CFD predictions and the experimental data on the two levels of measurement for temperature (High and Low) are shown in Table 6.

Table 6. Maximum deviation between the CFD predictions and experimental data [26].

Thermocouple Positions	Experimental Temperature (°C)	Predicted Temperature (°C)	% Deviation
High 1	1366	1230	9.95%
High 2	1264	1220	3.48%
High 3	1236	1119	3.47%
High 4	1239	1193	3.71%
Low 1	1320	1195	9.46%
Low 2	1277	1173	8.14%
Low 3	1225	1155	5.71%
Low 4	1206	1176	2.48%

5.2. Temperature and Efficiency

The operational lambda value has different major effects on the performance of a flameless oxyfuel burner. This magnitude is a controlling parameter in the operational program that can easily be adjusted by the operators. An increase of the lambda value, with a constant burner capacity (fuel mass rate) requires an introduction of more oxygen through the feeding nozzle. Considering the constant nozzle diameter and oxygen density for all the cases, this leads to a significant increment of the injection velocity of oxygen. This will highly affect the combustion mixing ratio and the eddy formations around the flame, and consequently the interaction of the gaseous mixture in forming IFGR. This aspect, which is a key feature of using flameless oxyfuel burners, influences the recirculation ratio, as well as the shape of the volumetric flame and the temperature profile inside the chamber. This magnitude also affects the thermal efficiency of the furnace, since it controls the total mass rate of the exhaust flue gases. Therefore, in order to investigate the effect of different lambda magnitudes on the temperature distribution inside the furnace, results from the validated CFD simulation have been studied. In this regard, the predicted results for the temperature distribution of six cases, with different lambda values (Table 3) are shown in Figure 6a,b. Each of these figures shows the gas temperature on a line that starts from the frontal wall and ends on the backend wall, on the left side (Figure 6a) and the right side (Figure 6b) of the chamber. The height of these lines are y = 2093 for Figure 6a (High level) and y = 1093 for Figure 6b (Low level). These heights are the same as the location for the High and Low thermocouples, as shown in Figure 4.

This observation shows that an increased lambda value, after reaching the stoichiometric ratio, decreases the global temperature inside the chamber. Results from case 1, when using a lambda value lower than 1, shows the lowest flue gas temperatures inside the furnace. This is due to an incomplete combustion. The maximum local temperature inside the chamber is seen for the case with a lambda value equal to 1.02 (case 2), which is the case with the closest lambda value to the stoichiometric amount. These results, which are in agreement with previous studies [30], indicate the destructive effect of an extra amount of oxygen on the thermal efficiency of the furnace. This is due to the fact that the heated extra oxygen increases the thermal losses through the exhaust gases.

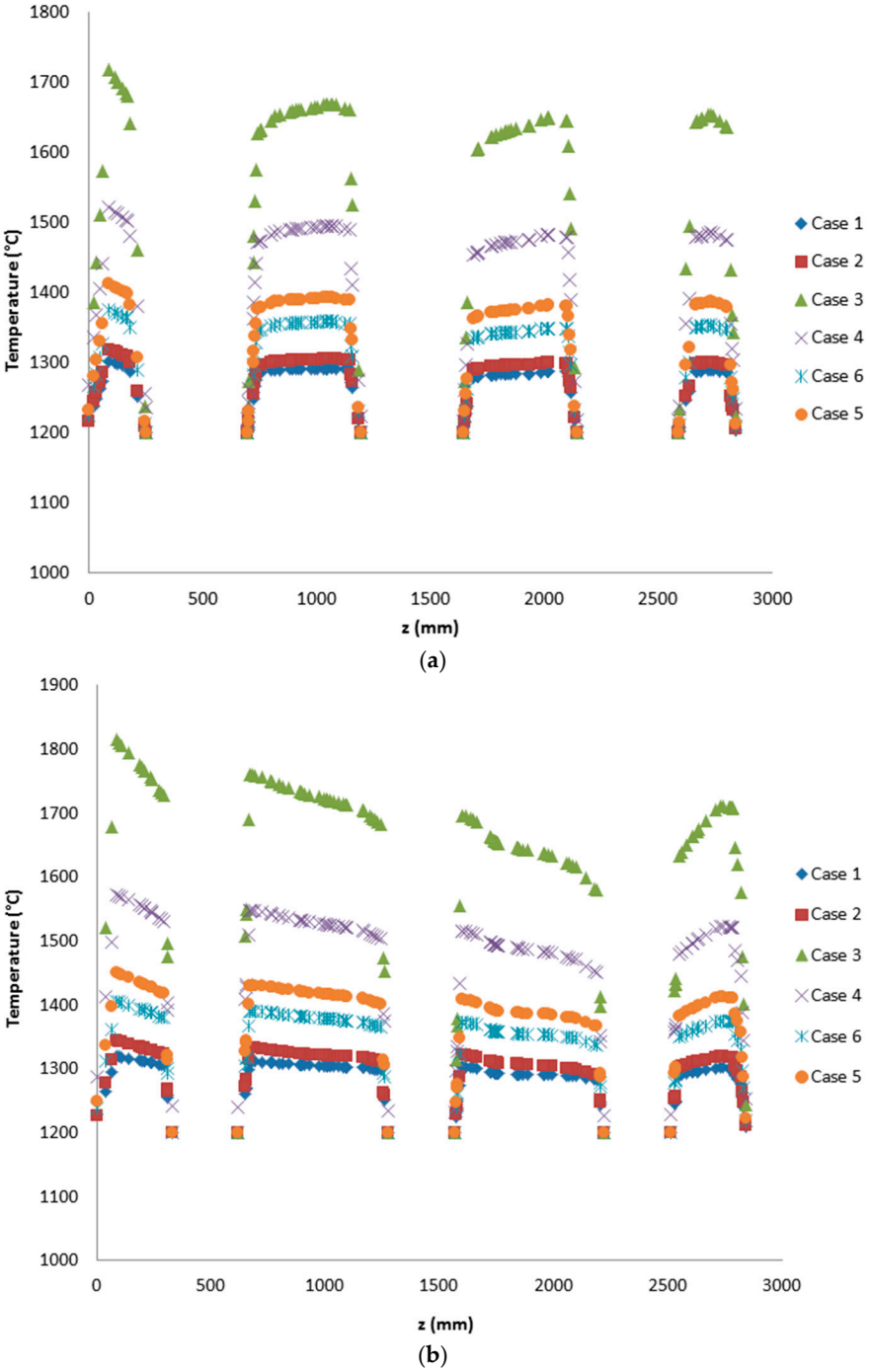

Figure 6. Temperature profile on *z*-*x* axis inside the furnace for all six studied cases: (**a**) High level with y = 2093; (**b**) Low level with y = 1093.

The energy balance inside the chamber can be expressed as follows:

$$Q_{in} = Q_{stock} + Q_{losses} + Q_{exhaust} \quad (13)$$

where Q_{in} stands for the total inlet thermal energy, and Q_{loss} is the summation of all the losses during the heating process. The parameter the $Q_{exhaust}$ value is defined as follows:

$$Q_{exhaust} = \dot{m}_{exhaust}\, C\, (T_s - T_g) \quad (14)$$

With an increased lambda value, $Q_{exhaust}$ increases due to an increment in the total exhaust gas mass rate and it decreases due to the lower final exhaust gas temperature. In order to picture the effect of these two variables, the final gas temperature, total exhaust gas mass rate, and the total $Q_{exhaust}$ are shown in Table 7 for all the studied cases, except for case 1. This table also shows the parameter $\%\Delta T$, which stands for the percentage of maximum temperature difference for these cases of study.

Table 7. Exhaust losses for cases 2, 3, 4, 5 and 6.

Case Number	Total Exhaust Gas Mass Rate	Exhaust Gas Temperature	$Q_{exhaust}$	$\%\Delta T$
	kg/s	°C	kW	
Case 2	0.058	1210	40.10	5.2%
Case 3	0.061	1300	44.52	14.9%
Case 4	0.060	1280	42.36	9.4%
Case 5	0.064	1230	39.72	6%
Case 6	0.069	1220	40.34	4.7%

On the other hand the lambda value (oxygen injection velocity) highly affects the temperature uniformity inside the chamber. This effect is well illustrated in Figures 7 and 8, which show the predicted temperature profile on a *z*-*y* and *x*-*z* surface in the middle of the furnace. The predicted results show a worse temperature uniformity of almost 28% for the lower lambda value (λ = 1.02) in case 3 compared to case 6 (λ = 1.2). It is also seen that case 5, with a lambda value equal to 1.1, retains the lowest exhaust loss.

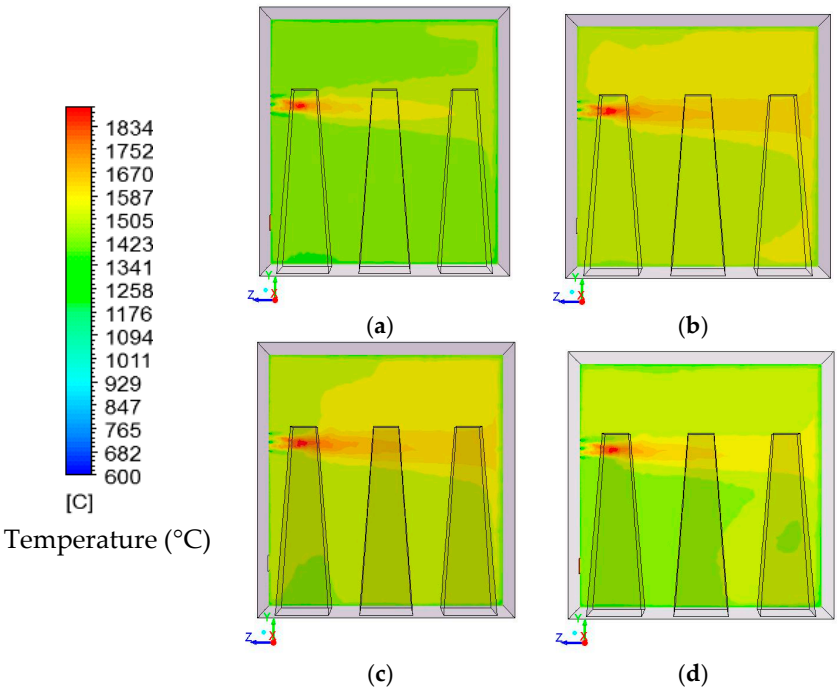

Figure 7. Predicted temperature (°C) profiles on a *z*-*y* surface in the middle of the furnace for selected cases: (**a**) Case 1; (**b**) Case 3; (**c**) Case 5; and (**d**) Case 6.

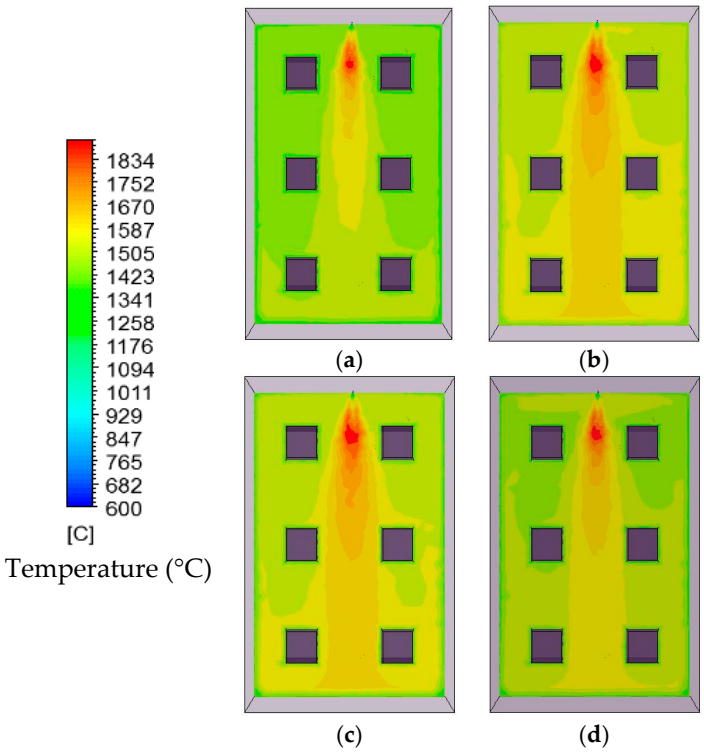

Figure 8. Predicted temperature (°C) profiles on a *x*-*z* surface in the middle of the furnace for selected cases: (**a**) Case 1; (**b**) Case 3; (**c**) Case 5; and (**d**) Case 6.

It can be argued that, even though the excess oxygen value reduces the overall thermal efficiency, it jeopardizes the uniformity of the temperature inside the chamber. This phenomenon is also argued by Scheele et al. [4] (p. 37) that explains the importance of using a high injection velocity to reach the ultimate operational conditions for such burners, especially in the absence of the FGR system. It is mentioned by Vesterberg et al. [23] that small nozzle diameters, for both fuel and oxygen and near sonic injection velocity, promises high IFGR. This in turn promotes the uniformity of the temperature inside the chamber. These factors are designed in order to compensate for the suppressed convective forces of the combustion products in oxy-fuel combustion, in comparison to the conventional air-fuel combustion systems [26].

Figure 8, illustrates the positive effect of an increased oxygen mass rate (injection velocity) on the formation of a volumetric flame shape and consequently a better temperature distribution. This is especially seen when comparing the results for case 6 and case 3. Specifically, the hot region of flue gases is widely distributed on the furnace height as the total temperature difference in case 3 is reported to be 272 (14.9%) while the amount for case 6 is 67 (4.7%).

It was previously shown by Ghadamgahi et al. [26] that the impinging effect of the flame contributes to a worse temperature uniformity. This phenomenon is considered imperceptible in this comparative study, for the sake of reducing the key parameters. This is observable from the results of this study (Figure 9), which shows the velocity magnitudes on a *z*-*y* surface in the middle of the furnace for two selective cases 1 and 3. It is seen that the flame impinges the rear wall in all the cases and that the increasing lambda value strengthens the impinging effect.

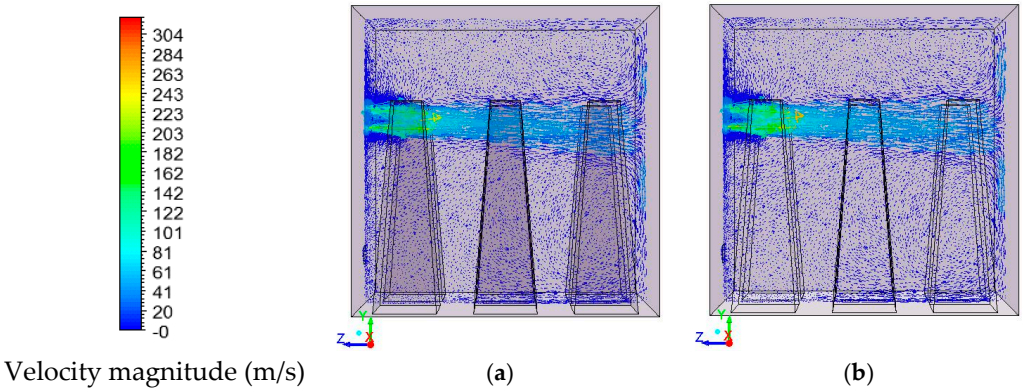

Figure 9. Velocity magnitude (m/s) profiles on a *z*-*y* surface in the middle of the furnace for selected cases: (**a**) Case 1 (λ = 0.95); (**b**) Case 3 (λ = 1.02).

The non-uniform temperature distribution largely affects the scale formation on the ingots. The regions with a higher local temperatures result in an increased level of oxidation and consequently a higher scale formation. The non-uniform scale formation on ingots in different positions inside the furnace and for one soaking heat treatment causes great financial losses in this production step. It also necessitates the need to define an on-line rolling force for each ingot in the rolling mill, which is the next step after the soaking process [26]. These losses that are consequences of operational conditions of the furnace must be considered. Especially when they result in large scrapping and scrapping loads, according to the production statistics in Ovako Sweden AB. In this regard, and in order to consider a factor that includes different aspects of losses in a furnace, the authors introduce a novel definition of the efficiency for a furnace. This definition considers the financial losses due to the non-uniformity in temperature and heat transfer distribution that causes scale formations and scrapping. Thus, the total financial losses may be expressed as follows:

$$Q\,loss_{total} = Q\,loss_{Thermal} + Q\,loss_{Production} \quad (15)$$

where $Q\,loss_{Production}$ is defined as a summation of the following losses:

- Losses due to a non-uniform scale formation
- Losses due to scrapping of ingots
- Losses due to a variable rolling process
- Furnace operational costs, such as damages on the lid due to a localized peak temperature.

and $Q\,loss_{Thermal}$ is defined as a summation of the following losses:

- Sensible heat of waste gases ($Q_{exhaust}$)
- Heat losses from the furnace surface
- An incomplete combustion of the fuel

In this study, the total thermal losses, except the exhaust losses, are assumed to be constant for all of the cases. The production losses on the other hand, are largely different due to a dissimilar combustion behavior and consequently a different temperature distribution and heat transfer ratio. This concept is illustrated in Figure 10 for the six cases of this study. The figure shows the total production losses and the exhaust losses in a comparative scheme. The production losses are estimated according to the existing statistical data from the rolling mill production site in Ovako Sweden AB.

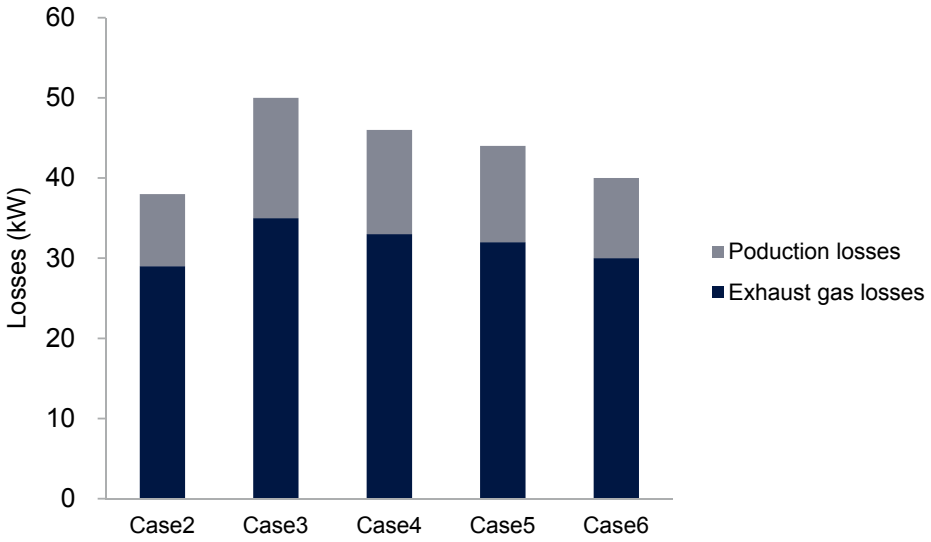

Figure 10. Exhaust and operational furnace losses for all the studied cases.

It is shown that even though case 3 retains the lowest thermal loss (lowest lambda values after the stoichiometric amount), it maintains a considerable amount of production losses in comparison to the other cases. This comparison indicates the importance of considering production losses, despite the fact that they used to be neglected in evaluating the furnace operational conditions as well as for the selection of a suitable combustion system.

6. Conclusions

A previously validated mathematical model was used to simulate the combustion and heat transfer in a soaking pit furnace, equipped with a flameless oxy-fuel burner. Simulations were done for six cases with different lambda values, starting from 0.95 to 1.2, and the predicted results were compared. The following conclusions were drawn:

- A good selection of models in the CFD calculations results in accurate predictions for the temperature, with a minimum deviation of 2.48% and maximum deviation of 9.46% compared to the experimental results. Specifically, to simulate a flameless oxyfuel combustion, it is necessary to consider the non-equilibrium effects during combustion and the non-gray effects of the radiative gases.
- A selection of the controlling parameters such as the lambda value has a major effect on the final operational conditions in flameless oxyfuel combustion systems. It is seen that by increasing the lambda value from 1.02 to 1.2 the exhaust losses increase, but also give a wider volumetric flame, thus a more uniform temperature distribution is obtained.
- The most thermally efficient lambda value ($\lambda = 1.02$) results in a worse temperature uniformity of 28%, compared to the case with a λ value of 1.2. The outcome of this drawback causes up to a 24% decrease in the production losses, such as the costs of a non-uniform scale formation, a non-uniform product quality, scrappings, and variable rolling forces.
- increase of the oxygen injection velocity by increasing the lambda value makes the hot region of flue gases more widely distributed on the furnace height, as the total temperature difference in case 3 ($\lambda = 1.02$) is 272 (14.9%) while the amount for case 6 ($\lambda = 1.2$) is 67 (4.7%).
- Comparing the predicted results for the temperature distribution profile for cases with different lambda values as the control parameter shows a significant difference between their operational losses and consequently their total furnace losses. The authors would like to encourage that this method be employed in industry while designing combustion systems and key operational parameterss, in order to avoid undesirable losses.

Acknowledgments: Special thanks go to Ovako Sweden AB for financing this research. In addition, we are very thankful to Marcus Svadling at Ovako Sweden AB for performing the temperature measurement trials at the plant, and Garry Wicks for helping with editing the language. Our colleagues Jun Li and Mohsen Saffari Pour are also greatly acknowledged for their help in this work. Also, special thanks to Henrik Häll for his support and help.

Author Contributions: Mersedeh Ghadamgahi and Nils Å. I. Andersson developed the CFD model, with the supervision of Pär Jönsson. The experimental work was supported by Patrik Ölund. The paper was written by Mersedeh Ghadamgahi with supervision of Pär Jönsson.

Conflicts of Interest: The authors declare no conflict of interest.

References

1. Chen, L.; Yong, S.Z.; Ghoniem, A.F. Oxy-fuel combustion of pulverized coal: Characterization, fundamentals, stabilization and CFD modeling. *Prog. Energy Combust. Sci.* **2012**, *38*, 156–214. [CrossRef]
2. Buhre, B.J.P.; Elliott, L.K.; Sheng, C.D.; Gupta, R.P.; Wall, T.F. Oxy-fuel combustion technology for coal-fired power generation. *Prog. Energy Combust. Sci.* **2005**, *31*, 283–307. [CrossRef]
3. Scheffknecht, G.; Al-Makhadmeh, L.; Schnell, U.; Maier, J. Oxy-fuel coal combustion—A review of the current state-of-the-art. *Int. J. Greenh. Gas Control* **2011**, *5*, S16–S35. [CrossRef]
4. Scheele, J.V.; Gartz, M.; Paul, R.; Lantz, M.T.; Riegert, J.P.; Söderlund, S. Flameless oxyfuel combustion for increased production and reduced CO_2 and NO_x emissions. *Stahl und Eisen* **2008**, *128*, 35–40.
5. Weller, A.E.; Rising, B.W.; Boiarski, A.A.; Nordstrom, R.J.; Barrerr, R.E.; Luce, R.G. *Experimental Evaluation of Firing Pulverized Coal in a CO_2/O_2 Atmosphere*; Argonne National Laboratory: Lemont, IL, USA, 1985.
6. Berry, G.; Wolsky, A. Modeling heat transfer in an experimental coal-fired furnace when CO_2/O_2 mixtures replace air. In Proceedings of the ASME Winter Annual Meeting, Anaheim, CA, USA, 7–12 December 1986.
7. Abele, A.R.; Kindt, G.S.; Clark, W.D.; Payne, R.; Chen, S.L. *An Experimental Program to Test the Feasibility of Obtaining Normal Performance from Combustion Using Oxygen and Recycled Gas Instead of Air*; Argonne National Laboratory: Lemont, IL, USA, 1987.
8. Wall, T.; Gupta, R.; Buhre, B.; Khare, S. Oxy-fuel (O_2/CO_2, O_2/RFG). In Proceedings of the 30th International Technical Conference on Coal Tilization & Fuel Systems, Clearwater, FL, USA, 17–21 April 2005.
9. Kim, H.K.; Kim, Y.; Lee, S.M.; Ahn, K.Y. NO reduction in 0.03–0.2 MW oxy-fuel combustor using flue gas recirculation technology. *Proc. Combust. Inst.* **2007**, *31*, 3377–3384. [CrossRef]
10. Andersson, K.; Normann, F.; Johnsson, F.; Leckner, B. NO emission during oxy-fuel combustion of lignite. *Ind. Eng. Chem. Res.* **2008**, *47*, 1835–1845. [CrossRef]
11. Toftegaard, M.B.; Brix, J.; Jensen, P.A.; Glarborg, P.; Jensen, A.D. Oxy-fuel combustion of solid fuels. *Prog. Energy Combust. Sci.* **2010**, *36*, 581–625. [CrossRef]
12. Ghadamgahi, M.; Ölund, P.; Ekman, T.; Andersson, N.; Jönsson, P. A comparative CFD study on simulating flameless oxy-fuel combustion in a pilot-scale furnace. *J. Combust.* **2016**, *2016*, 6735971. [CrossRef]
13. Wall, T.; Liu, Y.; Spero, C.; Elliott, L.; Khare, S.; Rathnam, R.; Zeenathal, F.; Moghtaderi, B.; Buhre, B.; Sheng, C.; et al. An overview on oxyfuel coal combustion—State of the art research and technology development. *Chem. Eng. Res. Des.* **2009**, *87*, 1003–1016. [CrossRef]
14. Johansson, R.; Andersson, K.; Leckner, B.; Thunman, H. Models for gaseous radiative heat transfer applied to oxy-fuel conditions in boilers. *Int. J. Heat Mass Transf.* **2010**, *53*, 220–230. [CrossRef]
15. Hjärtstam, S.; Johansson, R.; Andersson, K.; Johnsson, F. Computational fluid dynamics modeling of oxy-fuel flames: The role of soot and gas radiation. *Energy Fuels* **2012**, *26*, 2786–2797. [CrossRef]
16. Habermehl, M.; Erfurth, J.; Toporov, D.; Förster, M.; Kneer, R. Experimental and numerical investigations on a swirl oxy-coal flame. *Appl. Therm. Eng.* **2012**, *49*, 161–169. [CrossRef]
17. Galletti, C.; Coraggio, G.; Tognotti, L. Numerical investigation of oxy-natural-gas combustion in a semi-industrial furnace: Validation of CFD sub-models. *Fuel* **2013**, *109*, 445–460. [CrossRef]
18. Liu, C.C.; Ferng, Y.M.; Shih, C.K. CFD evaluation of turbulence models for flow simulation of the fuel rod bundle with a spacer assembly. *Appl. Therm. Eng.* **2012**, *40*, 389–396. [CrossRef]
19. Aziz, M.; Budianto, D.; Oda, T. Computational fluid dynamic analysis of co-firing of palm kernel shell and coal. *Energies* **2016**, *9*, 137. [CrossRef]
20. Filipponi, M.; Rossi, F.; Presciutti, A.; Ciantis, S.D.; Castellani, B.; Carpinelli, A. Thermal analysis of an industrial furnace. *Energies* **2016**, *9*, 833. [CrossRef]

21. Fredriksson, P.; Claesson, E.; Vesterberg, P.; Lugnet, A.; Ritzen, O. *Application of Oxyfuel Combustion in Reheating at Ovako, Hofors Works, Sweden—Background, Solutions and Results*; Linde AGA: Solna, Sweden, 2006.
22. Blasiak, W.; Yang, W.H.; Narayanan, K.; Von Scheele, J. Flameless oxy-fuel for fuel consumption and NO_x reduction and productivity increase. *J. Energy Inst.* **2007**, *80*, 3–11. [CrossRef]
23. Vesterberg, P.; Moroz, G. Flameless oxyfuel for highly visible results. In Proceedings of the AISTech 2006, Cleveland, OH, USA, 1–4 May 2006.
24. Krishnamurthy, N.; Paul, P.J.; Blasiak, W. Studies on low-intensity oxy-fuel burner. *Proc. Combust. Inst.* **2009**, *32*, 3139–3146. [CrossRef]
25. Krishnamurthy, N.; Blasiak, W.; lugnet, A. Development of high temperature air and oxy-fuel combustion technologies for minimized CO_2 and NO_x emission in industrial heating. In Proceedings of the Joint International Conference on "Sustainable Energy and Environment (SEE)", Hua Hin, Thailand, 1–3 December 2004.
26. Ghadamgahi, M.; Ölund, P.; Ekman, T.; Andersson, N.Å.I.; Jönsson, P. Numerical and experimental study on flameless oxy-fuel combustion in a pilot-scale and a real-size industrial furnace. *Appl. Therm. Eng.* **2017**. submitted.
27. Yin, C. Nongray-gas effects in modeling of large-scale oxy–fuel combustion processes. *Enertgy Fuels* **2012**, *26*, 3349–3356. [CrossRef]
28. Yang, W.; Blasiak, W. Numerical simulation of properties of a LPG flame with high-temperature air. *Int. J. Therm. Sci.* **2005**, *44*, 973–985. [CrossRef]
29. Ghadamgahi, M.; Ölund, P.; Lugnet, A.; Saffari Pour, M.; Yang, W. Design optimization of flameless-oxyfuel soaking pit furnace using CFD technique. *Energy Procedia* **2014**, *61*, 611–614. [CrossRef]
30. Habib, M.A.; Elshafei, M.; Dajani, M. Influence of combustion parameters on NO_x production in an industrial boiler. *Comput. Fluids* **2008**, *37*, 12–23. [CrossRef]